Available online at www.sciencedirect.com
ScienceDirect
International Journal of Fatigue 29 (2007) 1726–1736
International Journal of Fatigue
www.elsevier.com/locate/ijfatigue

Invited keynote paper

Fatigue history and in-situ loading studies of the overload effect using high resolution X-ray strain profiling

Mark C. Croft [a,b,*], Najeh M. Jisrawi [c,d], Zhong Zhong [b], Ronald L. Holtz [e], Kuntimaddi Sadananda [f], John R. Skaritka [b], Thomas Tsakalakos [c]

[a] Department of Physics and Astronomy, Rutgers University, Piscataway, NJ 08854-8019, United States
[b] National Synchrotron Light Source, Brookhaven National Laboratory, Upton, NY 11973, United States
[c] Ceramics Department, Rutgers University, Piscataway, NJ 08854, United States
[d] Department of Basic Sciences, University of Sharjah, P.O. Box 27272, Sharjah, United Arab Emirates
[e] Naval Research Laboratory, 4555 Overlook Avenue SW, Washington, DC 20375, United States
[f] Technical Data Analysis, Inc., Falls Church, VA 22046, United States

Received 4 October 2006; received in revised form 5 January 2007; accepted 15 January 2007
Available online 30 January 2007

Abstract

High-energy synchrotron X-ray diffraction experiments are used to perform local crack plane strain profiling of 4140 steel compact tension specimens fatigued at constant amplitude, subjected to a single overload cycle, then fatigued some more at constant amplitude. X-ray strain profiling results on a series of samples employing in-situ load cycling are correlated with the crack growth rate (da/dN) providing insight into the da/dN retardation known as the "overload effect". Immediately after the overload, the strain under maximum load is greatly reduced but the range of strain, between zero and maximum load, remains unchanged compared to the pre-overload values. At the point of maximum retardation, it is the strain range that is greatly reduced while the maximum-load strain has begun to recover to the pre-overload value. For a sample that has recovered to approximately half of the original da/dN value following the overload, the strain at maximum load is fully recovered while the strain range, though partially recovered, is still substantially reduced. The dominance of the strain range in the overload effect is clearly indicated. Subject to some assumptions, strong quantitative support for a crack growth rate driving force of the suggested form $[(K_{max})^{1-p}(\Delta K)^p]^\gamma$ is found. A dramatic nonlinear load dependence in the spatial distribution of the strain at maximum retardation is also demonstrated: at low load the response is dominantly at the overload position; whereas at high loads it is dominantly at the crack tip position. This transfer of load response away from the crack tip to the overload position appears fundamental to the overload effect for high R-ratio fatigue as studied here.

Keywords: Fatigue; Strain; X-ray; Synchrotron; Overload

1. Introduction

Attempts to quantitatively understand the growth rate of fatigue cracks in response to cyclic loading have a long history [1–3]. Since fatigue crack growth involves localized fracture at the crack tip, it depends intrinsically upon the local internal strain–stress fields and accumulated damage in the vicinity of the tip. The modeling work in this area has been carried forward with great resourcefulness despite the lack of clear, direct experimental data to provide fundamental guidance on these crucial local strain–stress fields. The purpose of this paper is to directly correlate variations in crack growth rate with variations in the local strains around the crack tip. The crack growth rate retardation after a single overload cycle in an otherwise constant amplitude fatigue experiment (see for example Fig. 1b) will serve as a vehicle for this comparison [4–7]. Understanding the important overload effect is also a first step in the

* Corresponding author. Tel.: +1 732 445 2524; fax: +1 732 445 4343.
E-mail address: croft@physics.rutgers.edu (M.C. Croft).

0142-1123/$ - see front matter © 2007 Elsevier Ltd. All rights reserved.
doi:10.1016/j.ijfatigue.2007.01.016

direction of understanding fatigue crack growth under arbitrary variable amplitude loading conditions.

Previously, we have described the ongoing development of high-energy synchrotron radiation X-ray diffraction techniques to map local strain fields in general [8], and in the vicinity of fatigue cracks in particular [9]. In this paper, we apply these techniques to a series of 4140 steel compact tension (CT) specimens which have been fatigued at constant amplitude, subjected to a single overload cycle then subsequently fatigued to various crack extensions beyond the overload point (see for example Fig. 1). The choices of samples and in-situ loading studies in this paper were based upon the measured crack growth rate curve specific to our samples, shown in Fig. 1b. For all of the samples, high spatial resolution measurements of the systematic variation of the ε_{yy} strain component in the crack plane, along a line spanning the crack tip position, have been made. Here, as in our previous work [9], the external load is applied along the y-direction. The crack plane was defined by $y = 0$; the crack tip is at $x = 0$, unless otherwise noted herein; and all measurements are made over a small gauge volume in the center ($z = 0$) of the CT plate. Following our previous work, we have substantially increased the spatial resolution of our strain measurements with the x–y cross-section of our gauge volume being routinely $50 \times 50\ \mu m^2$ in the vicinity of the crack tip. The data will show that such high resolution is essential to reveal some of the fine structural details of the strain fields in the vicinity of the crack tip.

We have also measured ε_{yy} profiles in-situ in the spectrometer with the CT samples under external (static) loads corresponding to various load levels in the constant amplitude, and overload cycle, fatigue processes. Specifically the changes in the strain profiles $\Delta\varepsilon_{yy}$ with changing load will be addressed here. This allows us to probe the crucial strain field response to these load levels before, during, after, and well-after the overload cycle. Mindful of the tri-axial character of the stresses in these systems we will assume, for initial interpretation purposes, that the behavior of the strains ε_{yy} and $\Delta\ \varepsilon_{yy}$ can be used as indicators of the behavior of the stresses σ_{yy} and $\Delta\sigma_{yy}$ and of the crack tip stress intensities K_{max} and ΔK.

2. Experimental materials and preparation

The samples used in this study are 4 mm thick 4140 steel compact tension (CT) specimens as described in Ref. [5]. The material is in the normalized condition and the specimen orientation is L-T. Crack length was measured via the dc potential drop method and ASTM E647 procedures. The fatigue preparations of the various samples are summarized schematically in Fig. 1. All specimens were first precracked to a crack length of 25.4 mm under constant amplitude fatigue conditions with: $K_{max} = 39.6$ MPa $m^{1/2}$; and $K_{min} = RK_{max}$ with $R = 0.1$. At the 25.4 mm crack length discussed here the corresponding applied load used to generate K_{max} was $F_{max} = 3.8$ kN. A test sample was

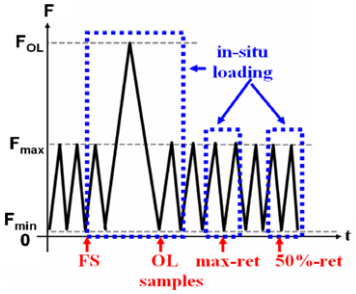

Fig. 1a. A schematic of loading sequence preparation for the specimens for this study The red arrows indicate the points where various samples were prepared by stopping in the fatigue sequence. The dotted rectangles indicate the regions in the fatigue process where in situ loading experiments were carried out. The max-ret and 50%-ret points occur, respectively at $\sim 6(10)^3$ and $\sim 2(10)^4$ cycles beyond the overload point. (For interpretation of the references in colour in this figure legend, the reader is referred to the web version of this article.)

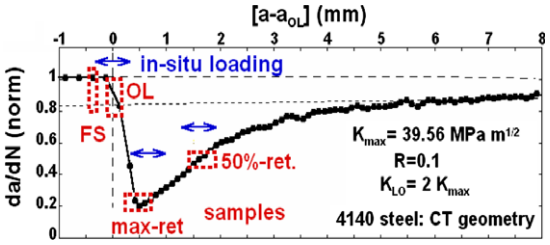

Fig. 1b. The crack growth rate da/dN plotted versus crack length, a, for a 4140 steel compact tension (CT) sample fatigued under constant amplitude conditions with an overload cycle. The crack length is referenced with respect to the crack length at overload $a_{OL} = 25.4$ mm and da/dN is normalized to the pre-overload crack growth rate of $2.05\ (10)^{-4}$ mm/cycle. The dotted boxes indicate the portion of the curve corresponding to the four specimens that were examined via EDXRD and the arrows indicating the regions where in-situ load experiments were carried out.

then subjected to an overload with $F_{OL} = 2F_{max}$ and subsequently fatigued again at constant $K = K_{max}$ to propagate the crack through the overload damaged region (see Fig. 1a for a schematic of this cycle sequence). The crack growth rate curve, da/dN (where N is the number of fatigue cycles) for this test sample is shown in Fig. 1b, normalized to the pre-overload crack growth rate. This da/dN curve shows the typical overload retardation affect [4–7]. This curve was used to estimate the crack lengths to which the cracks in subsequent samples should be grown in order to explore the strain fields corresponding to key points on the da/dN. A schematic of the samples prepared, and subsequent in-situ loading experiments is shown in Fig. 1a. The samples prepared were: a constant amplitude fatigue sample (denoted FS in the figure); a constant amplitude fatigue sample with a terminal overload cycle (denoted OL); and two samples which were fatigued, overloaded, and further fatigued to crack lengths corresponding to maximum da/dN retardation (denoted max-ret), and approximately 50% recovery to the pre-overload growth rate (denoted 50%-ret).

2.1. Experimental: synchrotron EDXRD

Details of the application of synchrotron based energy dispersive X-ray diffraction (EDXRD) to measurement of local strain fields in general [8] and in the vicinity of fatigue cracks were discussed in a previous articles by the authors [9]. Note that a review of the literature X-ray for strain analysis also appeared in these papers [8,9]. The technique exploits the high intensity, high-energy white beam (30–200 KeV) X-rays of the X17 wiggler beamline at the Brookhaven National Synchrotron Light Source. In EDXRD, the incident beam and detector remain fixed at the desired fixed scattering angle 2θ (with $2\theta = 12^\circ$ in our experiments). A spectrum simultaneously spanning a set of Bragg diffraction lines is collected using a solid-state Ge detector. The energy of a Bragg line, E_{hkl}, is related to the spacing, d_{hkl}, between of atomic planes in the material by the relation $E_{hkl} = 6.199/[\sin(\theta) d_{hkl}]$ where $\{hkl\}$ are the Miller indices identifying the crystalline planes, E_{hkl} is in KeV and d_{hkl} is in Å. Fitting a given Bragg line allows the precision determination of its center of gravity (in energy) and the calculation of the d_{hkl} lattice plane spacing. Variations in the atomic plane spacing from position to position in a specimen are then determined from the shifts in d_{hkl}, as determined from the Bragg line energy shift. In the strain variations reported here, the shifts of the most intense ($h = 3,\ k = 2,\ l = 1$) line were used. Using other Bragg lines, a statistical average of a collection of Bragg lines [8,9], or full pattern fitting procedures [10–12] produce similar results. The strain variation from position to position in the sample is then determined from the shifts in Bragg peak energy via the relation $\varepsilon_{hkl} = (\Delta d/d_0)_{hkl} = (\Delta E/E_0)_{hkl}$ as the sample is translated through the beam. Here $\Delta d = d - d_0$ is the change in the lattice plane spacing, d_0 is the lattice spacing of the stress-free materials, $\Delta E = E_0 - E$ is the corresponding Bragg peak shift and E_0 is the center of gravity of peak of the stress-free material [8,9]. A point far from the crack tip was chosen to determine the E_0 value. Measurements on Bragg lines with differing hkl yielded essentially identical results indicating that anisotropies in the strain (i.e., variations in ε_{hkl} with differing hkl) are not crucial in the problem/material at hand and the hkl subscript will be suppressed henceforth. Our previous work [8,9] involved both multiple and single Bragg line analysis. Recent synchrotron work by other groups mapping facets of the strain fields around fatigue cracks, differing from those presented in this paper, should also be noted [10–12].

The incident beam consists of highly parallel radiation that is tightly collimated to a cross-section as small as 50 μm × 50 μm near the crack tip. Further from the tip, where high-resolution is not crucial the slits were expanded to 100 μm parallel to the crack in order to increase the counting rates. The diffracted beam path was also highly collimated thereby defining a small gauge volume in the specimen over which the interatomic plane spacing was being measured. It is important to note that the stability of the rigidly fixed incident and scattering beam paths enables both the high spatial resolution of the strain variation in the specimen and the high precision determination of the interatomic spacings ($\Delta d/d$ less than ± 0.0001).

High spatial resolution measurements around fatigue cracks are greatly facilitated by indexing the in-situ position measurements to the fatigue crack itself. This crack based positioning is accomplished by measuring the beam intensity transmitted through the translated sample, and constructing a radiographic transmission profile. Such transmission profiles enabled precision location the crack and the crack tip in the X-ray beam. Uncertainties in the tip position were roughly ±0.05 mm.

Since X-ray diffraction methods measure inter-atomic spacings, our measurements are sensitive to elastic strain only, and not directly related to plastic deformations. In a sense, the inter-atomic spacings can be thought of as embedded local strain gauges which are "read" by X-ray diffraction. The presence of plasticity is evidenced by the local elastic strains in the absence of external load or the failure of the elastic strains to respond fully to an external applied load. Examples of both of these effects will be seen below.

In order to measure strain profiles of cracked specimens while under load in-situ, a fixture was constructed to open the crack mouths by using a jack screw. The load at the screw pivot point was measured by a digital Transducer Techniques load monitor. A typical strain profile at a given load would entail about 3 h data collection time.

3. Residual strains

Fig. 2 shows high resolution profiles of the residual (i.e., zero applied load) ε_{yy} strain component. These profiles are in the crack plane and along the crack propagation direction. The profile labeled FS and OL are, respectively for a constant amplitude fatigued specimen and a similarly fatigued specimen with a terminal overload of magnitude $F_{OL} = 2F_{max}$.

The point labeled 1 in the figure lies in the wake zone behind the crack tip. The presence of a narrow region adjoining the crack flanks, where ε_{yy} manifested a sharp negative anomaly, was noted in a previous work by the authors [9]. Subsequent work has clearly shown that this wake region is characterized by a strong anisotropy with ε_{xx} manifesting a sharp positive anomaly. The region labeled 2 in the figure marks a positive upturn in ε_{yy} which is consistently observed upon approaching the crack tip from the crack ($x < 0$) direction.

The features labeled 3 indicate the process zone plastic region in the vicinity of the crack tip. In the inset of Fig. 2, an expanded view offers a better picture of the large-negative-peak strain anomaly, characteristic of the process zone. In the constant amplitude fatigued case (FS), the crack tip is just before the sharp drop in ε_{yy}, which marks the entrance into the process zone, and the width of the process zone feature is approximately 0.15 mm (see figure inset). In the case

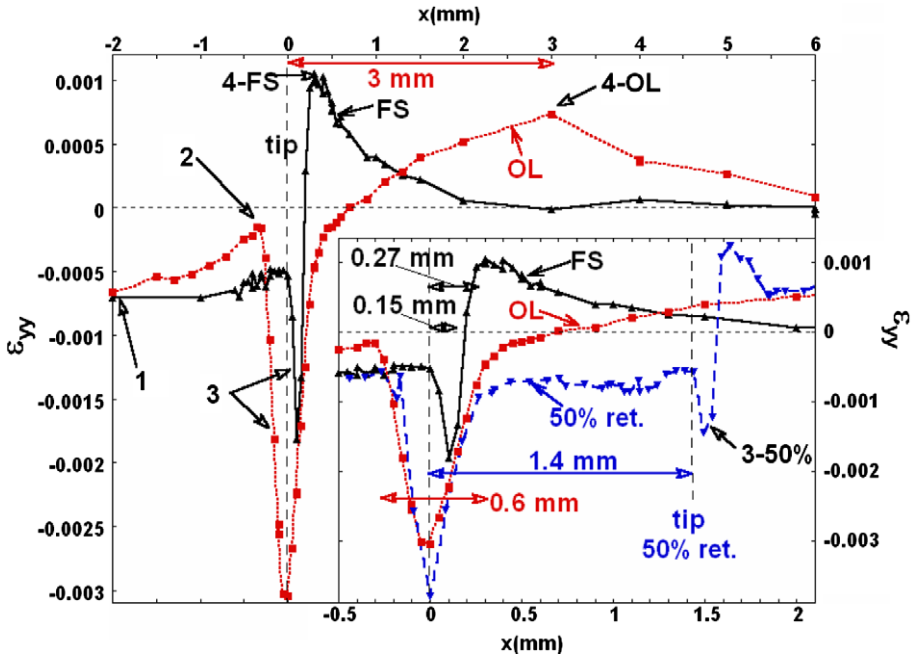

Fig. 2. The residual ($F = 0$) ε_{yy} strain profiles for: the constant amplitude fatigued sample (FS), the fatigued sample with an overload (OL) of magnitude $F_{OL} = 2F_{max}$, and the 50%-ret sample. The first two profiles are in the main part of the figure, and are shown again an expanded view in the inset with the 50%-ret profile included. Unless otherwise stated in this and subsequent figures, the following conventions are followed: the crack tip is at $x = 0$ with the crack extending in the $x < 0$ direction; and the strain profiles are along the crack propagation direction (x) and in the $y = 0$, crack plane. In order to illustrate the movement of the crack tip through the OL induced strain field in this figure only the 50%-ret strain profile has been displaced to align the OL feature at $x = 0$ and the crack tip is at $x = 1.4$ mm.

of the overload sample (OL), the crack tip was determined to be in the center of the very large OL process zone feature, and the width of the process zone has expanded to about 0.6 mm.

The residual ε_{yy} strain profiles exhibit a maximum labeled 4-FS and 4-OL in the figure for the constant amplitude and overload cases, respectively. These points mark the farthest extent in front of the crack tip of the monotonic plastic zone and occur at distances of about 0.27 mm and 3.0 mm for the constant amplitude and overload cases, respectively. The spatial extent of the monotonic plastic zone is approximately equal to the spatial extent of the overload crack growth retardation effect (see Fig. 1b). This is consistent with long standing notions that the retardation ceased as the crack tip exited the monotonic plastic zone [4–7]. Beyond the monotonic zone the residual strain is presumed to be elastic.

In the inset of Fig. 2 we have also included the residual ε_{yy} strain profile for the post overload sample, for which the crack growth rate has recovered to approximately 50% of the pre-overload rate (the 50%-ret sample). In this case, the crack tip position has been displaced to $x \sim 1.4$ mm and the overload position has been aligned at $x = 0$ to coincide with the original OL sample overload position. Interestingly, the overload feature for the 50%-ret sample is not only equal in strength but actually appears somewhat stronger than in the original OL sample. In view of the fact that these are different samples, and that the overload feature decreases rapidly in amplitude if one moves slightly away from the crack plane [9] the differences in the overload feature will be neglected here. The process zone feature for the 50%-ret sample is at $x \sim 1.5$ mm (labeled 3–50%) and can be seen to closely resemble the feature for the constant amplitude case. This is consistent with the substantial recovery of the strain fields in the vicinity of the crack tip in this well-after-overload sample.

3.1. In-situ load sequence through overload

Fig. 3 shows the ε_{yy} strain profiles for a fatigued sample cycled in-situ through a fatigue cycle (between $F = 0$ and F_{max}), an overload cycle (to $F = F_{OL} = 2F_{max}$), and a post overload cycle (between $F = 0$ and F_{max}). The dwell time to collect the diffraction data at each point in the load cycle was approximately 3 h. The residual ($F = 0$) strains profiles have been discussed at length above so we will concentrate on the overload cases here.

As mentioned in the introduction, we assume that the behavior of the measured elastic strains ε_{yy} (and $\Delta\varepsilon_{yy}$) can be used as an indicator of the behavior of the full internal stresses σ_{yy} (and $\Delta\sigma_{yy}$). Moreover, we assume that the extrapolation/evaluation of ε_{yy} and $\Delta\varepsilon_{yy}$ to/at the position of the crack tip can be used to infer the behavior of the crack growth parameters K_{max} and ΔK. Hence, the very important observation that the magnitude of ε_{yy} at $F = F_{max}$ after the overload [ε_{yy}(am) in figure] is dramatically suppressed with respect to the ε_{yy} at $F = F_{max}$ before the overload [ε_{yy}(am) in figure]. Namely, it argues in favor

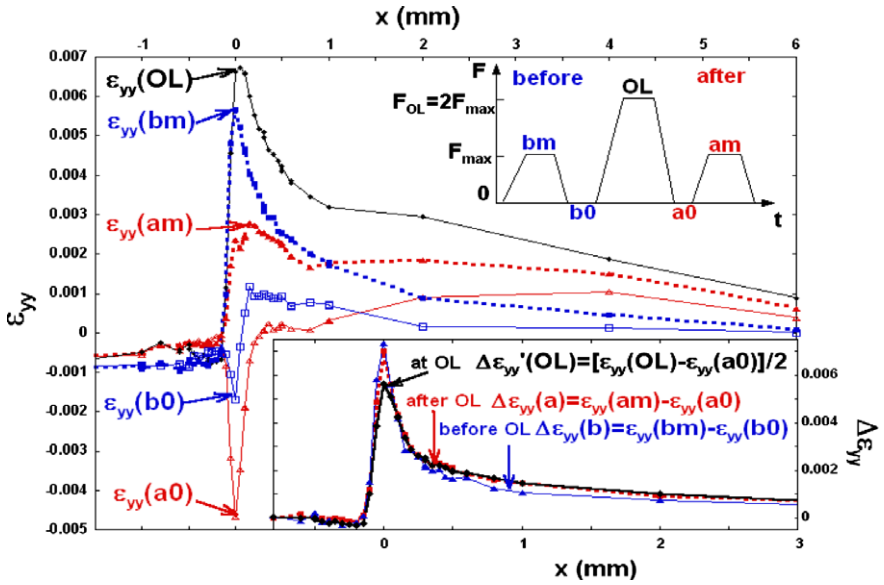

Fig. 3. The ε_{yy} strain profiles for a constant amplitude fatigued sample before, during, and after an overload cycle. The load sequence (applied load, F, versus time, t) is illustrated in the upper inset schematic. The fact that this data was collected with statically applied loads has been emphasized in this schematic by the flat tops and bottoms on the saw-tooth load curve. The strain profiles shown are for: the before overload $F = F_{max}$ (bm) and $F = 0$ (b0) conditions; the after overload $F = F_{max}$ (am) and $F = 0$ (a0) conditions; as well as the $F = F_{OL} = 2F_{max}$ (OL) condition. Inset (lower) This inset shows a series of strain ranges: $\Delta\varepsilon_{yy} = [\varepsilon_{yy}\ (\text{at}F = F_{max}\ ) - \varepsilon_{yy}\ (\text{at}F = 0)]$ for both the before overload (b) and after overload (a) conditions; and the overload $\Delta\varepsilon'_{yy}(OL) = [\varepsilon_{yy}\ (\text{at}\ F = F_{OL}) - \varepsilon_{yy}\ (\text{at}\ F = 0\ \text{at}\ a0)]/2$. In the case of $\Delta\varepsilon'_{yy}(OL)$ it should be noted that the strain range has been divided by a factor of two because the applied load $F_{OL} = 2F_{max}$ and it was desired to compare to the other strain ranges obtained at the load of F_{max}.

of an immediate suppression of the stress at the tip and the parameter K_{max} after the overload. While the presence of the residual stresses after an overload has made this suppression of K_{max} expected on theoretical grounds our experimental results provide very real and direct support for it as well as an estimate of its relative magnitude.

Under load, the ε_{yy} strain profiles for both the $F = F_{max}$ and $F = F_{OL}$ cases show large enhancements approaching the crack tip from the front (the positive x-direction). Under an external force, the purely elastic stress component, σ_{yy}, manifests a $x^{-1/2}$ singularity approaching the crack tip from the front and its conjugate strain would be expected to reflect similar behavior. Of course residual stresses and/or plastic deformation will modify this singular behavior. In fact the residual stresses present before and after the applied load cause a very substantial deviation from pure elastic singular behavior. As will be seen below, however, the strain range, in which the residual strain is subtracted, does appear to manifest the singular functional form over a reasonable length scale.

3.2. Strain range response before, after and during the overload

Since the crack tip growth driving force depends upon both K_{max} and ΔK [13], it is useful to consider also the quantitative load induced changes in the ε_{yy} profiles. Accordingly in the lower inset in Fig. 3 we show the difference (or strain range) profiles, $\Delta\varepsilon_{yy}$, obtained by subtracting the $F = 0$ curve from the $F = F_{max}$ curves displayed in the main part of Fig. 3. Both the before, $\Delta\varepsilon_{yy}(b)$, and after $\Delta\ \varepsilon_{yy}(a)$, overload strain ranges are displayed. In addition a $\Delta\varepsilon'_{yy}(OL)$ curve is also shown in the inset of Fig. 3. For $\Delta\varepsilon'_{yy}(OL)$ it was assumed that the residual strain after the overload was created by the overload application and that therefore $\Delta\varepsilon'_{yy}(OL) = [\varepsilon_{yy}(OL) - \varepsilon_{yy}(a0)]/2$. This is equivalent to treating the overload cycle ($F = F_{OL}$ to $F = 0$) on the same basis as the constant amplitude ($F = F_{max}$ to $F = 0$) cycles. The additional factor of 1/2 in the definition of $\Delta\varepsilon'_{yy}(OL)$ is to account for the fact that $F_{OL} = 2F_{max}$ (rather than just F_{max}) for the purpose of comparison to the other $\Delta\varepsilon_{yy}$ curves obtained with $F = F_{max}$. Note that here, and in the data analysis below, spline fitting of the data to define a continuous function for subtraction purposes was used, when needed, for calculating differences in ε_{yy} profiles. All data points shown on the curves were actual data collection points of either (or both) the loaded or residual strain profile.

It is important to note that both the maximum amplitude and the overall x-dependence of the strain range $\Delta\varepsilon_{yy}$ curves are almost identical before $[\Delta\varepsilon_{yy}(b)]$ and after $[\Delta\varepsilon_{yy}(a)]$ the overload cycle. Indeed, with the above defined normalization, the behavior of $\Delta\varepsilon'_{yy}(OL)$ closely resembles the other $[\Delta\ \varepsilon_{yy}]$ curves except for some plasticity induced rounding of the peak at the crack tip position. Again assumption that behavior of $\Delta\varepsilon_{yy}$ provides an indicator of the behavior of $\Delta\sigma_{yy}$, leads to the inference that the $\Delta\ \varepsilon_{yy}$ behavior at the tip should reflect the behavior of the ΔK fatigue parameter. Hence, the fact that $\Delta\ \varepsilon_{yy}$ is essentially unchanged immediately after the overload suggests that

ΔK behaves similarly. On the other hand, $\Delta\varepsilon_{yy}$ will be seen to be suppressed after crack growth beyond the overload. This will suggest that while ΔK is undiminished immediately after the overload, it is suppressed after subsequent crack growth beyond the overload.

3.3. Singular behavior in the strain range response

As alluded to above, purely elastic response predicts an $x^{-1/2}$ behavior in the stress, where x is the distance from the crack tip. However, deviations from this would be expected in real materials due to plasticity of the crack tip. By considering $\Delta\varepsilon_{yy}$ one subtracts the residual strain and looks only at the material's local response to the imposed force. In the case at hand, we will look for linear behavior as x approaches zero (the crack tip), in $\Delta\varepsilon_{yy}^{-2}$ plotted versus x in order to test for $\sim x^{-1/2}$ type scaling [see Ref. [14]].

Additionally, two effects preclude looking for this singular behavior too far in front of the tip. First, in the compact tension (CT) geometry there is a node in σ_{yy} and consequently a linear far field strain, passing through zero, far in front of the tip. Secondly, small variations in the choice of the zero stress inter-atomic lattice spacing, which are a negligible fraction of the large near-tip strains, could make large fractional contributions in the far field. Referring to the data in Fig. 3, the strain field magnitude and nonlinear curvature is suggestive of $\sim x^{-1/2}$ behavior for x less than about 2.5 mm.

Fig. 4 shows $\Delta\varepsilon_{yy}^{-2}$ versus x plots for the same three cases, plotted in Fig. 3-inset; the before-OL [$\Delta\ \varepsilon_{yy}$(bm)] case, the before-OL [$\Delta\ \varepsilon_{yy}$(am)] case, and the at-OL[$\Delta\varepsilon'_{yy}$(OL)] case. In Fig. 4 the $\Delta\varepsilon_{yy}^{-2}$ behavior both before (b) and after (a) the overload appears to be linear with x (for x somewhat below 1.2 mm) as the crack tip is approached (see the dashed lines and the figure illustrating the scaling behavior). Despite the very large residual stress after the overload, the $\Delta\varepsilon'_{yy}(\mathrm{OL})^{-2}$ plot also manifests scaling behavior over a larger x-range (up to $x \sim 2$ mm). Interestingly the $\Delta\varepsilon'_{yy}(\mathrm{OL})^{-2}$ plot also superimposes with the $\Delta\varepsilon_{yy}(\mathrm{am})^{-2}$ plot as the crack tip is approached. This behavior is not surprising in view of the fact that the $\Delta\varepsilon'_{yy}$(OL) and $\Delta\varepsilon_{yy}$(am) curves in Fig. 3-inset superimpose for wide ranges of x. Thus, it appears that the elastic singular behavior approaching the crack tip from the front is reflected in the change in ε_{yy} induced by the applied external load.

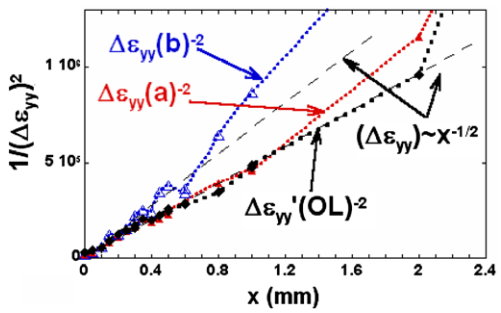

Fig. 4. Plots of $1/\Delta\varepsilon_{yy}^2$ versus x in the region just in front of the crack tip where a square root singularity in the purely elastic behavior is anticipated. $\Delta\varepsilon_{yy} = [\varepsilon_{yy}(\mathrm{at}F = F_{max}) - \varepsilon_{yy}(\mathrm{at}F = 0)]$ for both the before (b) and after (a) overload conditions. In addition the at-overload strain range $1/\Delta\varepsilon'_{yy}(\mathrm{OL})^2$ is plotted.

3.4. Maximum retardation sample strain response to load

In Fig. 5 the ε_{yy} strain profiles for the max-ret sample for loads of $F = 0$, F_{max}, and $F_{max}/2$ are shown. As expected, the F_{max} profile manifests a large positive ε_{yy} peak at the crack tip. In contrast, the $F = 0$ profile shows a strong negative peak at the position where the $2F_{max}$ overload (OL) was applied, with only a small peak type structure in the vicinity of the tip position. The intermediate load $F_{max}/2$ profile shows a dramatic decrease in the OL strain feature along with a more modest positive displacement (relative to the $F = 0$ profile) in the tip region.

3.5. Strain range response: maximum retardation sample

In the inset of Fig. 5, we show the strain range profiles, $\Delta\ \varepsilon_{yy}$, obtained by subtracting various curves in Fig. 5. The "$\Delta\varepsilon_{yy}$ for ΔF_{tot}" curve represents the x-dependence of the shift in the ε_{yy} strain between $F = 0$ and $F = F_{max}$. The $\Delta\varepsilon_{yy}$ for ΔF_{tot} curve very clearly manifests two strong positive peaks, one at the overload x-position, and one at the crack tip x-position. There is also a longer range falloff in this strain range in front of the crack tip.

The data in Fig. 5 makes it possible to break down the strain range response into contributions from a lower-range applied force change, ΔF_{low} (from $F = 0$ to $F = F_{max}/2$), and from a higher-range applied force change, ΔF_{high} (from $F = F_{max}/2$ to $F = F_{max}$). The strain range response in the low force region (see "$\Delta\varepsilon_{yy}$ for $\Delta\ F_{low}$" in figure) shows a dramatic peak at the overload x-position with a longer range falloff in the positive x-direction. In particular it should be noted that there is no strong feature in the strain range low force response at the crack tip position. Interestingly, the strain range response in the high force region (see "$\Delta\ \varepsilon_{yy}$ for ΔF_{high}" in figure) shows a similarly dramatic peak, now located at the x-position of the crack tip with a longer range falloff beyond the tip. There is no strong feature in the strain range high force response at the overload x-position. Thus, our results support a bifurcation in load response: between $F = 0$ and $F = F_{max}/2$ the strain range response is dominated by modifications in the OL spatial region; whereas between $F = F_{max}/2$ and $F = F_{max}$, the strain range response is dominated by modifications at the crack tip.

Motivated by the striking disparity observed in the low versus high load strain response, we have performed a more detailed sequence of strain profiles at various load levels (see Fig. 6). Due to beam time constraints, these profiles were collected with somewhat lower spatial resolution (e.g., $60 \times 60\ \mu m^2$ x–y cross-section and $\sim$500 μm extent in the z-depth direction). In the figure, the OL feature is seen

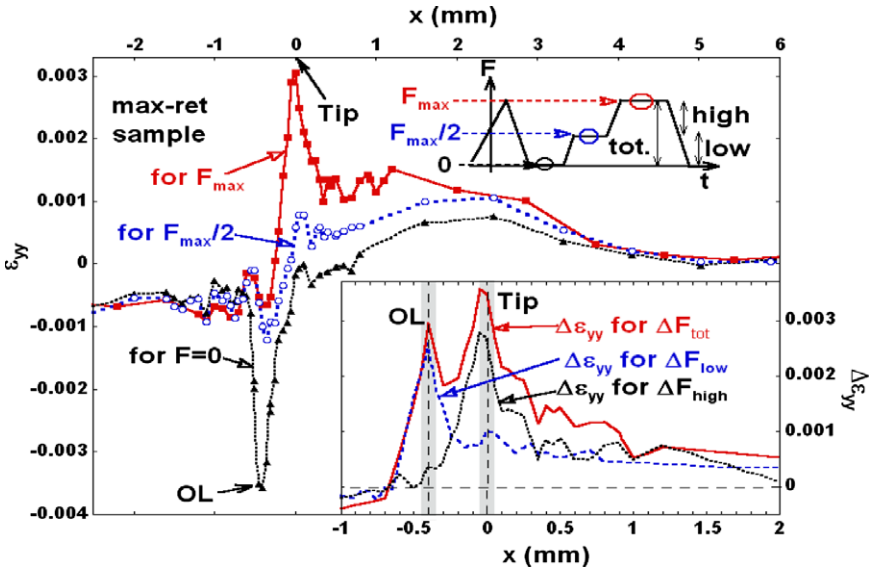

Fig. 5. The ε_{yy} strain profiles for the max-ret sample for zero external load ($F = 0$), for the maximum constant amplitude load fatigue load F_{max}, and for $F_{max}/2$. The positions at which the overload (OL) was applied and of the crack tip are indicated. The inset illustrates the load points in the fatigue cycle where the data was collected. Note that this data was collected with statically applied loans. Inset: the "differential" strain profiles $\Delta\ \varepsilon_{yy}$ for the max-ret sample obtained by subtracting the ε_{yy} profiles at different loads shown in the main figure. Specifically: for the "$\Delta\varepsilon_{yy}$ for ΔF_{tot}" case the $F = 0$ curve was subtracted from the $F = F_{max}$ curve; for the "$\Delta\varepsilon_{yy}$ for ΔF_{low}" case the $F = 0$ curve was subtracted from the $F = F_{max}/2$ curve; and for the "$\Delta\varepsilon_{yy}$ for ΔF_{high}" case the $F = F_{max}/2$ curve was subtracted from the $F = F_{max}$ curve.

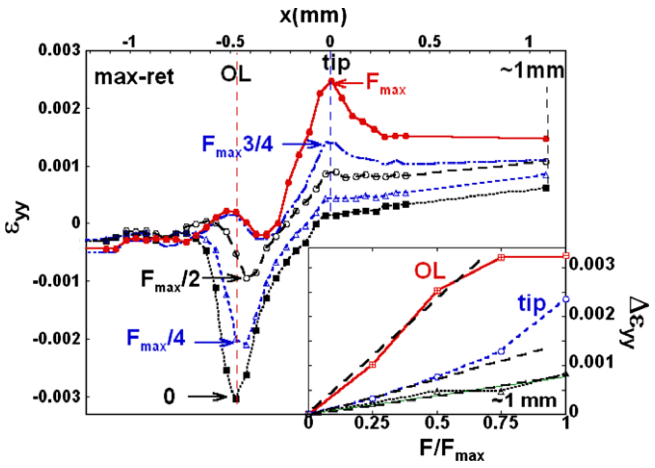

Fig. 6. A series of strain profiles (measured at somewhat lower spatial resolution) at five load levels between $F = 0$ and $F = F_{max}$. Dashed lines indicate the OL and tip positions as well as a position ~1 mm beyond the tip. Inset: the strain range, relative to the zero load strain versus load for these three positions.

to be rapidly suppressed under load and evolves from a sharp negative peak at $F = 0$, toward a modest positive and negative peak pair at high load. At the tip position, the peak-feature response onsets nonlinearly at loads above $F_{max}/2$.

The load induced strain range, (with respect to the $F = 0$ strains) at the OL, tip, and ~1 mm positions are plotted versus fractional load in the inset of Fig. 6. The ratios of the low load responses (see dashed lines in the figure) are 1:2:6.5 at the ~1 mm, tip, and OL positions, respectively. The high-load strain range clearly saturates at a limit at the OL position while it is enhanced at the tip position. These results illustrate in detail how the strain field response switches with applied load, i.e., the OL-region dominates the response at low-load; and the crack tip region dominates at higher loads. Inferring the behavior of the stress fields from these elastic strain behaviors, it appears that the stress concentration at the crack tip is reduced at low loads due to the dominant role of the OL region. Furthermore, at high loads, the influence of the OL region is diminished as the crack tip stress fields become dominant. Thus, these results indicate a nonlinear load dependent transfer of stress concentration between the OL region and the crack tip region is associated with the post overloading behavior.

3.6. 50% Retardation sample strain and strain range response to load

Fig. 7 shows a plot of the ε_{yy} strain profiles for the 50%-ret. sample in the cases of zero load ($F = 0$), and of $F = F_{max}$. As a reminder, this is a specimen that was subjected to an overload, then further fatigued with the constant pre-overload amplitude, and finally the fatiguing was stopped when da/dN had recovered to about 50% of its baseline value. Thus, this specimen represents effects midway between full retardation and baseline fatigue. The strain range, $\Delta\varepsilon_{yy}$, computed, as usual, by subtracting the $F = 0$ profile from the $F = F_{max}$ profile also is shown. The overload feature at $x \sim -1.4$ mm is prominent in the residual ($F = 0$) strain profile and is suppressed in the loaded $F = F_{max}$ profile. Consequently the strain range, $\Delta\varepsilon_{yy}$, manifests a large peak at the overload position. This is reminiscent of the behavior of the max-ret sample but

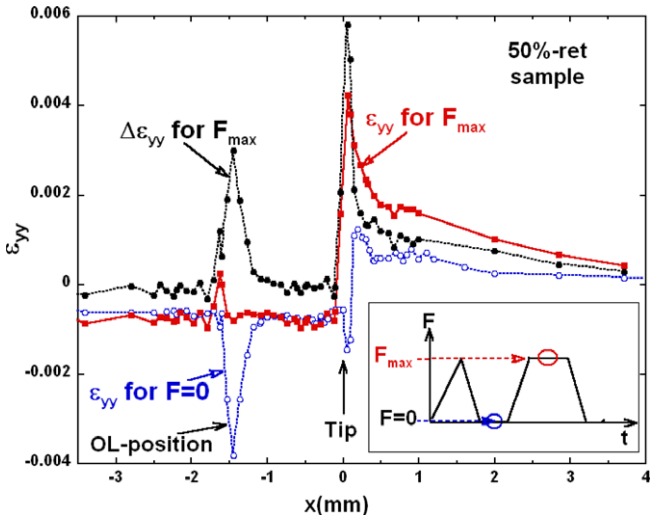

Fig. 7. The ε_{yy} strain profiles for the 50%-ret. sample, for zero external load ($F = 0$), and for $F = F_{max}$. Also shown is the strain range profile $\Delta\varepsilon_{yy}$. The inset shows a schematic of the applied load, F, versus time, t, and identifies the load points where the data were collected.

with the overload feature now displaced far enough from the tip feature to be totally resolved. It should be noted that the sharp structure in $\Delta\varepsilon_{yy}$ near $x = -1.6$ mm appears to result from experimental data scatter, amplified by subtracting the two curves.

4. Comparison of samples

We will now draw together and compare our strain profile results on the various samples under various load conditions. In Fig. 8a we compare the ε_{yy} residual ($F = 0$) strain profiles of the various pre-and post-overload samples studied here, with the convention that the crack tip is at $x = 0$. The overload strain feature is characterized by a large negative peak in ε_{yy} and this feature moves from $x = 0$ (for the immediately after overload curve), to $x \sim -0.4$ mm (for the max-ret curve), and to $x \sim -1.4$ mm (for the 50%-ret curve) as the crack tip progressively propagates farther from the OL point. As previously noted, the process zone anomaly of the 50%-ret has almost recovered the same characteristic narrow negative anomaly in ε_{yy}, observed for the before-OL sample. This is readily apparent here by their superposition.

In Fig. 8b we plot together the ε_{yy} strain profiles under the load of $F = F_{max}$ for the before-OL, after-OL, max-ret, and 50%-ret samples/conditions. In addition, ε_{yy} strain profile under the OL of $F = F_{OL} = 2F_{max}$, is included for reference. The large suppression of the ε_{yy} strain from before the overload to immediately after the overload is obvious in these curves. The slow recovery of the ε_{yy} strain upon moving from the after-OL, to the max-ret and still further to the 50%-ret conditions can also be seen. The values of these curves at the local maximum, near the crack tip (i.e., near $x = 0$), will be referred to below.

In Fig. 8c, we plot the $\Delta\varepsilon_{yy}$ strain range profiles for the before-OL, after-OL, max-ret, and 50%-ret samples/conditions. Several points should be noted here: (1) there is no change between the $\Delta\varepsilon_{yy}$ curves before and immediately after the overload; (2) the max-ret $\Delta\ \varepsilon_{yy}$ curve is both dramatically suppressed relative to the before-OL curve, and has one peak at the crack tip position and another at the overload position; (3) there is a recovery (near the crack tip position) in the 50%- ret $\Delta\varepsilon_{yy}$ curve toward the behavior of the before-OL curve and the OL peak is well separated from the crack tip peak.

Since local stress acting at the crack tip controls the crack propagation rate, we plot in Fig. 9 the values of $\varepsilon_{yy}(F = 0)$, $\varepsilon_{yy}(F = F_{max})$, $\Delta\ \varepsilon_{yy}$ ($F = 0$ to $F = F_{max}$) and ε_{yy}(ave) obtained from the local maxima of the curves (near $x = 0$) in the previous three figures. For reference the single point at $\varepsilon_{yy}(F = F_{OL})$ is also plotted. (Here the crack length relative to the overload position was measured both from the strain field data and by microscopy.) The immediate suppression of $\varepsilon_{yy}(F = F_{max})$ by the overload with a slow

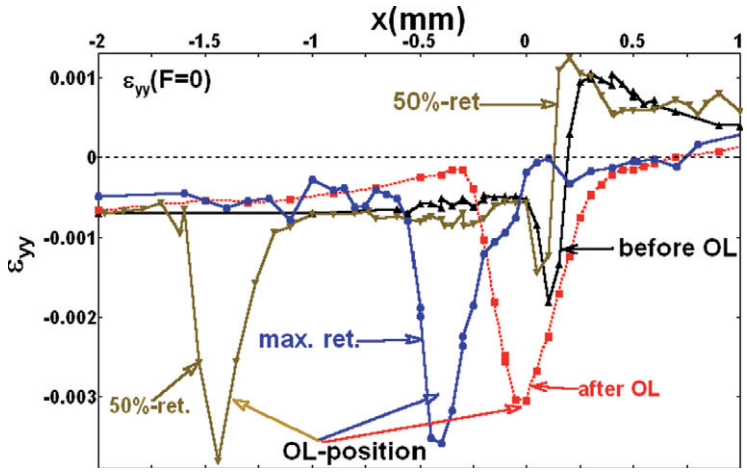

Fig. 8a. A comparison of the ε_{yy} residual ($F = 0$) strain profiles for the before-OL, after-OL, max-ret. , and 50%-ret. samples/conditions. The position of the OL feature can be seen to move progressively behind the propagating tip.

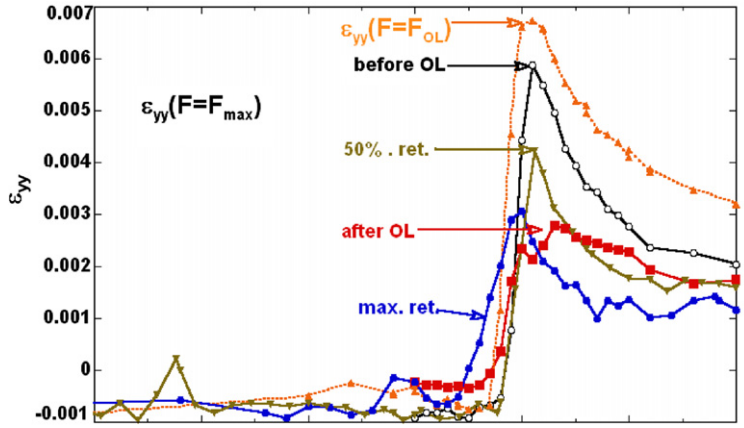

Fig. 8b. A comparison of the ε_{yy} strain profiles under the load of $F = F_{max}$ for the before-OL, after-OL, max-ret, and 50%-ret. samples/conditions. The ε_{yy} strain profile under the OL of $F = F_{OL} = 2F_{max}$ is included for reference. Note that the local maxima of these curves (near $x = 0$) will be used in the discussion which follows. (Not the x-axis is the same as in Figs. 8a and 8c).

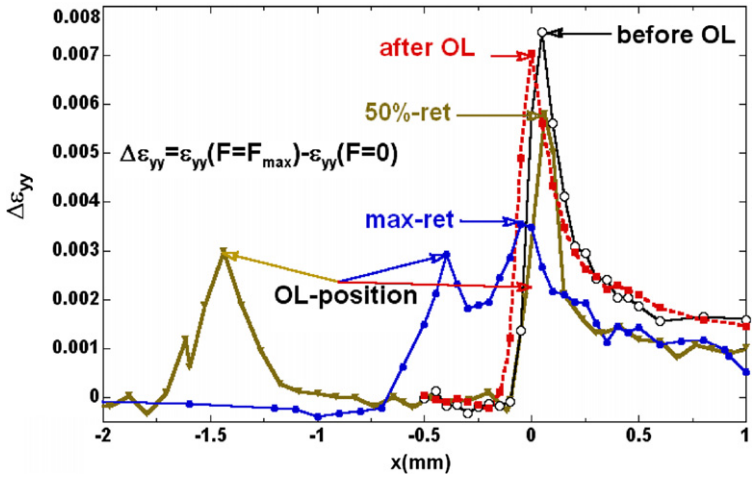

Fig. 8c. A comparison of the $\Delta\varepsilon_{yy}$ strain range profiles for the before-OL, after-OL, max-ret, and 50%-ret samples/conditions. Note that the local maxima of these curves (near $x = 0$) will be used in the discussion which follows.

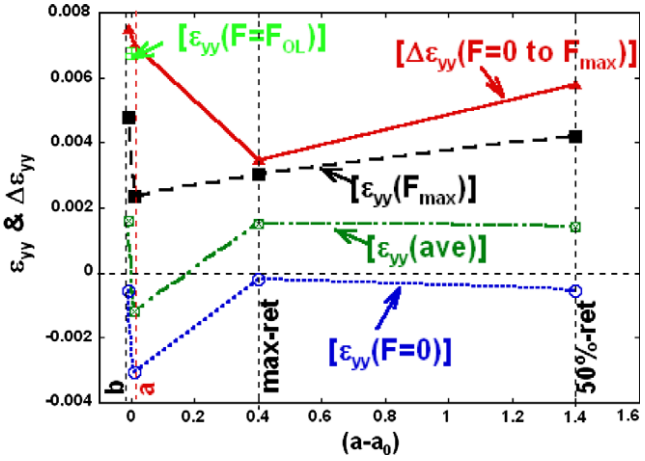

Fig. 9. A summary of the near-crack-tip values of $\varepsilon_{yy}(F = 0)$, $\varepsilon_{yy}(F = F_{max})$, $\Delta\varepsilon_{yy}(F = 0$ to $F = F_{max})$, $\varepsilon_{yy}(F = F_{OL})$ and $\varepsilon_{yy}(\text{ave}) = \{\varepsilon_{yy}(F = F_{max}) + \varepsilon_{yy}(F = 0)\}/2$ plotted versus crack tip position, measured relative to the overload.

recovery can be seen. The immediate introduction of a large negative strain after the overload in the residual $\varepsilon_{yy}(F = 0)$ strain is clear, along with the rather rapid recovery to nearer pre-overload levels. Finally, the delay in the suppression of the $\Delta\varepsilon_{yy}(F = 0$ to $F = F_{max})$ curve until the maximum retardation condition with a subsequent recovery should be noted. In order to compare fractional changes in these quantities we will, in what follows, normalize them to the values they had immediately before the overload.

4.1. Potential strain field result insights into the OL crack growth retardation effect

We now wish to summarize our strain field measurements in a way that might shed additional light on the retardation of crack growth produced by the overload. Fig. 10 shows an expanded plot of the normalized crack growth rate shown in Fig. 1b. This normalized curve makes immediately visible the fractional magnitude of the OL

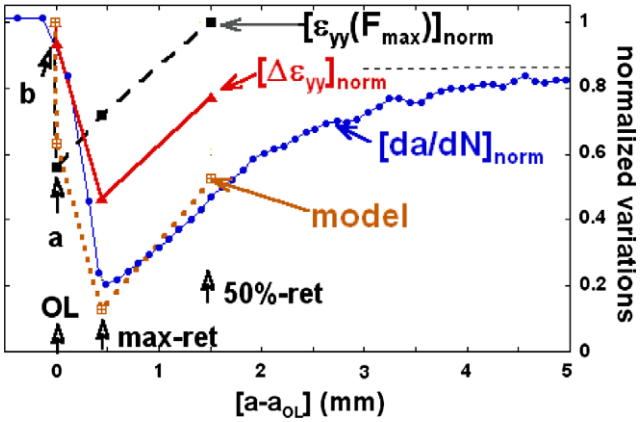

Fig. 10. A superposition of the crack growth rate da/dN and the at-crack-tip values of $\varepsilon_{yy}(F_{max})$, and of the strain range $\Delta\varepsilon_{yy}$. The values for these parameters are plotted for the before-OL (b), after-OL (a), max-ret, and 50%-ret samples/conditions. The abscissa is the crack length referenced with respect to the overload point. All of the ordinate values have been normalized to those just before the overload so that fractional changes can be compared (hence the label "norm" applied to all of the variables). Also plotted is the "model" expression $[\{[\varepsilon_{yy}(F_{max})]_{norm}\}^{1-p}\{[\Delta\varepsilon_{yy}]_{norm}\}^{p}]^{\gamma}$ with $p = 0.83$ and $\gamma = 3$ [12].

retardation effect, compared to the constant amplitude rate. The crack growth rate OL effect in our case is not "ideal" in the sense that it does not quite recover to the pre-overload rate far beyond the overload point. This experimental effect is not uncommon and will not be addressed here.

Fig. 9 displayed the experimental values of ε_{yy}(at $F = F_{max}$) and $\Delta\varepsilon_{yy}$(between $F = 0$ and $F = F_{max}$) at the position of the crack tip plotted versus the crack length. The values of these crack tip strains have been normalized to their values before the overload point in order to provide the fractional changes in the strain parameters, as a function of proximity to the overload position. The data for the normalized values of ε_{yy}(at $F = F_{max}$) {labeled $[\varepsilon_{yy}(F_{max})]_{norm}$ *in the figure*}, *and* $\Delta\varepsilon_{yy}$(between $F = 0$ and $F = F_{max}$) {labeled $[\Delta\varepsilon_{yy}]_{norm}$ in the figure} at various crack lengths are superimposed with the normalized da/dN curve plotted in Fig. 10.

For the purpose of discussion, we follow the proposal of Noroozi et al. [2] who characterized the crack growth rate driving force with the expression $da/dN \propto \alpha[(K_{max})^{1-p}(\Delta K)^{p}]^{\gamma}$. Here p and γ are derived from materials constants; i.e., are not empirical fit parameters. For 4140 steel specimens studied here, the estimates of $p = 0.83$ and $\gamma = 3$ have been made [15]. Our experiments have of course measured only the local strains but, as noted above, we posit that the behavior of ε_{yy} and $\Delta\varepsilon_{yy}$ are indicators of σ_{yy} and $\Delta\sigma_{yy}$ behavior. Therefore, when ε_{yy} and $\Delta\varepsilon_{yy}$ are evaluated at the tip position, they are indicators of the behavior of the crucial parameters K_{max} and ΔK. Proceeding on this assumption, a series of observations and inferences can be made.

Referring to Fig. 10, the most striking correlation is that between the position and magnitude of the overload induced anomaly in da/dN and the magnitude and position of the dip in the $[\Delta\varepsilon_{yy}]_{norm}$ points. This strongly supports the dominant contribution of the $(\Delta K)^{p}$ to the overload retardation effect. Moreover, noting that $[\Delta\ \varepsilon_{yy}]_{norm}$ was essentially unchanged immediately after the overload and manifests a delayed depression, correlates with the delay in the overload da/dN retardation effect. The inference here is that the delay in the suppression of ΔK causes the delay in the overload da/dN anomaly. Similarly, the fact that $[\varepsilon_{yy}(F_{max})]_{norm}$ is immediately depressed after the overload, whereas the da/dN anomaly onsets more slowly, is consistent with the $(K_{max})^{1-p}$ term playing a relatively minor role in the crack growth driving force.

Encouraged by these qualitative correlations, it is worthwhile taking the comparison one step further by comparing the full expression $[\{[\varepsilon_{yy}(F_{max})]_{norm}\}^{1-p}\{[\Delta\varepsilon_{yy}]_{norm}\}^{p}]^{\gamma}$, *with* $p = 0.83$ and $\gamma = 3$, to the $[da/dN]_{norm}$ in Fig. 10. The overall striking agreement between this trial expression and the crack growth rate behavior is probably fortuitously good in view of the assumptions made and the limitations of the experimental data. The disparity between the model and the data immediately after the overload (caused by the large effect in $[\varepsilon_{yy}\ (F_{max})]_{norm}$) should be noted. Nevertheless, pending continued critical model assessment and more detailed experimental work the agreement appears highly supportive of the fundamental modeling methods being applied by G. Glinka and coworkers.

5. Conclusions

This paper clearly demonstrates that synchrotron-based EDXRD measurements are eminently suitable for mapping the local strain fields in the vicinity of fatigue crack tips. Moreover, the small spatial scales and in-situ load dependences probed by this technique provide substantial insight into the fundamental understanding of fatigue crack growth. The direct correlation of the experimental fatigue crack growth rate (da/dN) after an overload, with the evolution of the near-crack-tip strain fields has been crucial in this study. Near the crack tip, immediately after the overload, the maximum strain is strongly suppressed while the strain range remains unchanged. For a sample fatigued after OL, to the maximum retardation condition, the strain range is dramatically suppressed, whereas the maximum strain has begun to recover. Thus, the overload retardation effect appears dominated by the strain range and, by inference, ΔK. Indeed, quantitative support for the crack growth rate modeling of Glinka et al. [15], which is also dominated by ΔK, has been shown. For the sample exhibiting maximum retardation, a dramatic nonlinear load-dependence in the spatial distribution of the strain has been demonstrated. Specifically, for loads less than about 0.7 F_{max} the strain field response is dominantly at the overload position, whereas at loads greater than this, the strain field response is dominantly at the crack tip position. Thus, this transfer of load response, away from the crack tip and to the overload position, appears fundamental to the overload

retardation effect for loading with high R ratios, where low loading is a significant portion of the fatigue cycle.

Acknowledgements

The authors gratefully acknowledge the support of the Office of Naval Research (ONR) under Contract No. N00014-04-1-0194 and also DURIP ONR N00014-02-1-0772. Utilization of the NSLS was supported by US Department of Energy Contract DE-AC02-76CH00016. The authors express their gratitude to Dr. A.K. Vasudevan for suggesting this materials problem and for a wealth of advice on the course of these studies. The authors acknowledge detailed conversations with G. Glinka and D. Kujawski on this work. The authors also thank N. Croft for useful suggestions on this manuscript.

References

[1] Paris PC, Erdogan F. A critical analysis of crack propagation laws. Trans ASME, J Basic Eng 1963;D85:528–34.
[2] (see) Noroozi AH, Glinka G, Lambert S. Int J Fatigue 2005;27:1277.
[3] Vasudevan AK, Sadananda K, Glinka G. Int J Fatigue 2001;23:S39. and References therein.
[4] Sadananda K, Vasudevan AK, Holtz RL, Lee EU. Int J Fatigue 1999;21:S233.
[5] Lang M, Marci G. Fatigue Fract Eng Mater Struct. 1999;22:257.
[6] See for example Suresh Subra. Fatigue of materials. NY: Cambridge University Press; 1998 (p. 305–6).
[7] Verma B, Ray PK. Bull Mater Sci 2002;25:301. of nondestructive evaluation 17 (1998) 129).
[8] Croft M, Zakharchenko I, Zhong Z, Gulak Y, Hastings J, Hu J, et al. J App Phys 2002;92. and References therein.
[9] Croft M, Zhong Z, Jisrawi N, Zakharchenko I, Holtz RL, Gulak Y, et al. Int J Fatigue 2005;27:1409. and References therein.
[10] Preuss M, Rauchs G, Doel T, Steuwer A, Bowen P, Withers PJ. Acta Materialia 2003;51:1045–57.
[11] James M, Hattingh D, Hughes D, Wei L-W, Patterson E, Quinta Da Fonseca J. Fatigue Fract Eng Mater Struct 2004;27:609.
[12] Steuwer A, Santisteban JR, Turski M, Withers PJ, Buslaps T. Nuclear Instruments and Methods in Physics Research B 2005;238:200–4.
[13] Vasudevan AK, Sadananda K, Louat N. Mater Sci Eng 1994;A188:1–22.
[14] Note that this data presentation method is similar to that typically used to emphasize the $1/(T - T_c)$ singularity (within mean field theory) in the magnetic susceptibility of a ferromagnet at temperatures (T) above its transition temperature (T_c). Namely, plotting the inverse susceptibility versus temperature yields a linear plot vanishing at T_c. For a discussion see:) Kittel C. Introduction to solid-state physics. fifth ed. N.Y.: John Wiley and Sons; 1976 (p. 459–60).
[15] G. Glinka, private communication.